Structural disorder and magnetism of the semiconducting clathrate $Eu_8Ga_{16}Ge_{30}$

B.C. Chakoumakos*, B.C. Sales, D.G. Mandrus

Solid State Division, Oak Ridge National Laboratory, Oak Ridge, TN 37831-6393, USA

Abstract

The temperature dependence of the atomic displacement parameters for an isotopically enriched $Eu_8Ga_{16}Ge_{30}$ crystal determined from refinements of neutron diffraction data show the anomalously large values for the Eu atom in the large cage persist from 295 to 12 K. The Eu site in the large cage is modeled by splitting it into four fractionally occupied positions, displaced 0.4 Å from the cage center. Fourier maps of this Eu site support this view in showing residual nuclear density with distinct peaks in the directions of the split-atom positions, and lesser density at the cage center position. The Ga and Ge atoms appear to be fully disordered on the three distinct framework sites. In comparing the isostructural $X_8Ga_{16}Ge_{30}$ (X=Eu, Sr, Ba) compounds, the positional disorder around the large cage site increases progressively with decreasing size of the caged atom. Below 35 K, $Eu_8Ga_{16}Ge_{30}$ orders ferromagnetically, with the preferred direction of the Eu moments along (100). The projected saturation value of the Eu moment, 7 μ_B, equals the free ion value. © 2001 Elsevier Science B.V. All rights reserved.

1. Introduction

Clathrate-type compounds [1–7] of the group IV elements [8], are providing new directions for thermoelectric materials research. Compounds isotypic with the type I hydrate structure $X_8(H_2O)_{46}$ of the ice clathrates (Fig. 1) [9] are of particular interest, because they exhibit cubic crystal structures, a generous range of solid solution, n-type semiconducting behavior, relatively high Seebeck coefficients and electrical conductivity, and glass-like thermal conductivity [7,10–13]. Recent X-ray structural studies of various clathrates of this type and related ones are expanding the range of known substitutions and revealing new structural variants; see for example Refs. [14–16] and references therein. Those with the structural formula X_8E_{46} can have E=Si, Ge, Sn, Al, Ga, In, and X=Na, K, Rb, Cs, Sr, Ba, Eu [7,8,10]. Here we compare and contrast the anomalously large 'rattling' of the guest atom in the oversize XE_{24} cage in the $X_8Ga_{16}Ge_{30}$ (X= Ba, Sr, Eu) compounds by means of neutron crystallography, reporting new structural results for $Eu_8Ga_{16}Ge_{30}$ and $Ba_8Ga_{16}Ge_{30}$, and explore how the structural disorder

effects transport properties for evaluating thermoelectric behavior. In a companion paper [17], we report heat capacity and magnetic, electrical and thermal transport measurements for single crystals of $X_8Ga_{16}Ge_{30}$ (X=Ba, Sr, Eu).

2. Experimental

For the $Eu_8Ga_{16}Ge_{30}$ single-crystal growth, about 2 g of Eu-153 metal initially were reduced from several fragments of a EuO crystal. Stoichiometric amounts of the Eu-153 metal, Ga shot (99.999%) and Ge (99.9999%) were loaded in a helium dry box into a carbonized silica tube. The tube was sealed under high vacuum, placed in a furnace and heated to completely melt the charge, cooled at 1–2°C/min to 625°C, held at 625°C for several days, and finally furnace cooled to room temperature. The resulting boule consisted of large (5–10 mm) single crystal grains of $Eu_8Ga_{16}Ge_{30}$. The $Ba_8Ga_{16}Ge_{30}$ crystals were grown by a similar recipe, except that $BaGe_2$ was first prepared by arc-melting Ba (99.999%) and Ge (99.9999%), then combined with the Ga in the carbonized silica tube, and the charge was cooled to 900°C. Several single crystals of the appropriate size (typically 2×2×2

*Corresponding author.

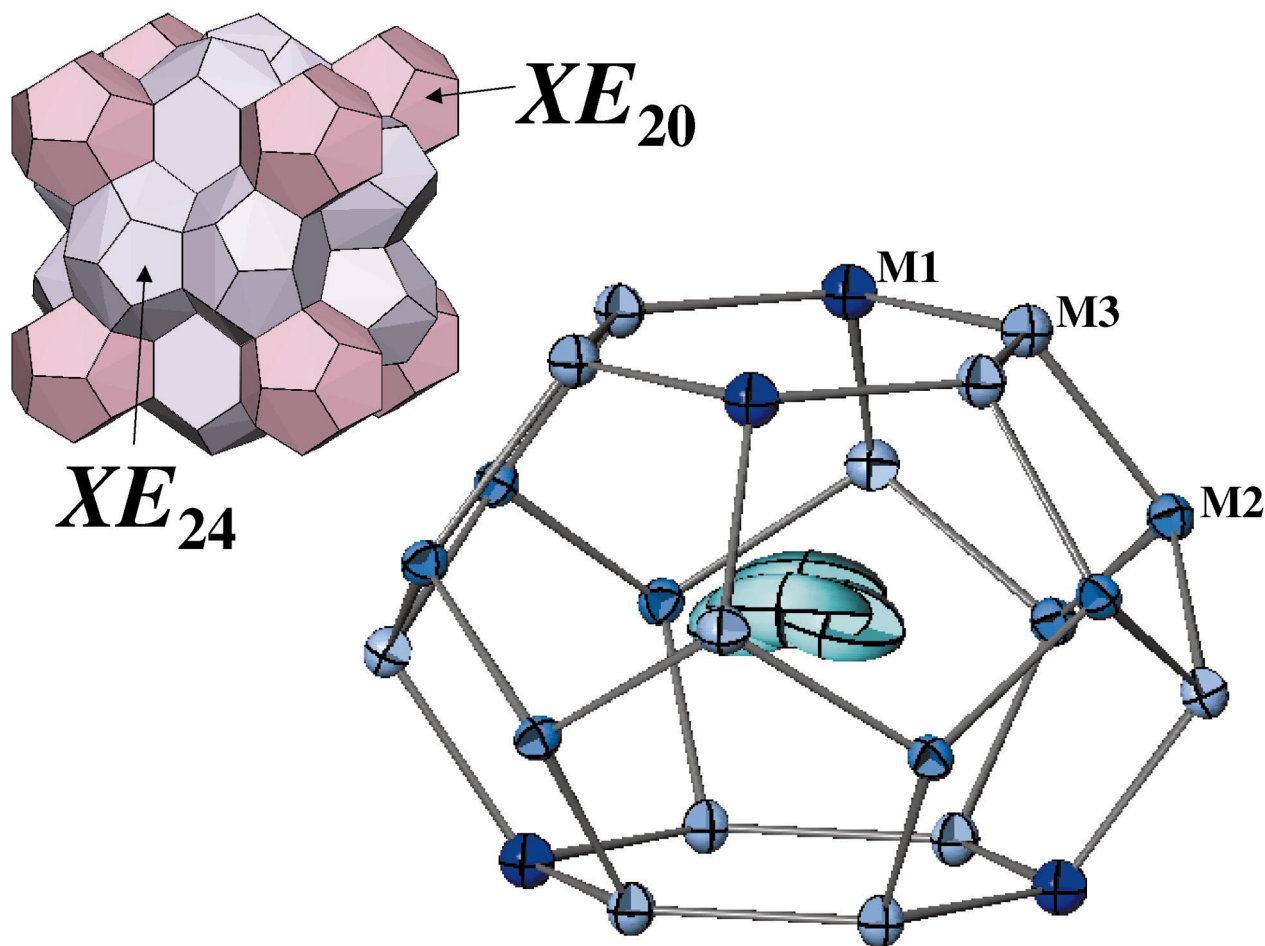*E-mail address:* kou@ornl.gov (B.C. Chakoumakos).

Fig. 1. (a) Space-filling polyhedra of the Type I hydrate clathrate structure adopted by the group IV elements. The crystal data are space group $Pm\bar{3}n$ with the structural formula $X_8E_6E_{10}E_{30}$ where E=Si, Ge, Sn, Al, Ga, In; X=Na, K, Rb, Cs, Eu, Ba. (b) Anisotropic atomic displacement probability densities for the Eu2 in the 24k split-site positions of the large polyhedral cavity. Ellipsoids are drawn for 99% probability.

mm^3) were sawn from the boules to be used for neutron diffraction.

For $Eu_8Ga_{16}Ge_{30}$, single-crystal neutron diffraction data were collected at 295, 200, 160, 120, 80, 40, 25, and 12 K using the HB2a four-circle diffractometer at the HFIR. For $Ba_8Ga_{16}Ge_{30}$, data were collected at 295, 225, 155, 85, and 15 K. The 331 reflection from a Ge monochromator at a take-off angle of 45° was used, which gives the neutron wavelength of 1.0037(2) Å for this instrument configuration. Sawn parallelepipeds, 1.75×1.82×1.95 mm^3 ($Eu_8Ga_{16}Ge_{30}$) and 1.5×1.75×2.25 mm^3 ($Ba_8Ga_{16}Ge_{30}$), each were glued to an aluminum pin and mounted on the cold-tip of a closed-cycle He refrigerator, which is mounted on the diffractometer and used to control the temperature. For data collection at each temperature the same set of 22 reflections was used for refining the lattice parameter and determining the orientation matrix. The data collections were carried out by radially scanning through the Ewald sphere. Generally, at each temperature a 1/16 sphere of Bragg reflections was measured with l=0–16 and $k \geq h$ to sin Θ/λ=0.763 Å^{-1}, except for the low temperature data sets of the $Eu_8Ga_{16}Ge_{30}$ for which,

inadvertently, only l=1–16 were recorded. Three reflections were monitored to correct the intensities for variations in the neutron flux, which did not vary by more than 1% for the duration of each data collection. The reflection intensities were integrated using the Lehmann–Larson algorithm and corrected for the Lorentz effect with the UCLA Crystallographic Software (C. Strouse, personal communication). For complete isotopic enrichment by Eu-153, the linear neutron attenuation factor for $Eu_8Ga_{16}Ge_{30}$, including both incoherent scattering and absorption, is 1.25 cm^{-1}, which gives μr=0.12 for the crystal used. For $Ba_8Ga_{16}Ge_{30}$ the linear neutron attenuation factor is 0.059 cm^{-1}, which gives μr=0.01 for the crystal used. Given these small values for μr, no absorption corrections were made. Neglecting a significant absorption correction would lead to underestimating the atomic displacement parameters (ADPs). We are justified in neglecting the absorption correction in these cases, because the ADPs of the host lattice atoms for both $Ba_8Ga_{16}Ge_{30}$ and $Eu_8Ga_{16}Ge_{30}$ turn out to be essentially the same. The GSAS software package [18] was used for the nuclear and magnetic structure refinements. The intensities of equivalent reflec-

Table 1
Refinement results for $Ba_8Ga_{16}Ge_{30}$, $Pm\bar{3}n$, $Z=1$, from neutron single-crystal diffraction data[a]

Temperature (K)	15	85	155	225	295
Measured reflections	1394	1394	1406	1406	1451
Independent reflections	448	449	452	453	463
Reflections with $I>3\sigma(I)$	255	242	246	243	231
$R(F)$	0.051	0.059	0.054	0.053	0.046
$wR(F^2)$	0.097	0.104	0.097	0.096	0.085
Goodness-of-fit, S	1.564	1.656	1.586	1.580	1.278
Extinction coefficient ($\times 10^{-5}$)	9(1)	8(1)	8(1)	8(1)	8.2(9)
Cell a (Å)	10.760(1)	10.755(1)	10.766(1)	10.774(1)	10.785(2)
$\rho_{calc.}$ (g/cm^3)	5.854	5.862	5.844	5.831	5.814
U_{eq} (Ba1) (Å^2)	0.003(1)	0.005(1)	0.008(1)	0.011(1)	0.010(1)
U_{eq} (Ba2) (Å^2)	0.014(2)	0.023(3)	0.028(3)	0.034(3)	0.038(3)
U_{eq} (M1) (Å^2)	0.005(1)	0.005(1)	0.007(1)	0.009(1)	0.009(1)
U_{eq} (M2) (Å^2)	0.0036(5)	0.0047(7)	0.0066(6)	0.0078(6)	0.0079(6)
x (M2)	0.1845(1)	0.1845(1)	0.1845(1)	0.1846(1)	0.1844(1)
U_{eq} (M3) (Å^2)	0.0042(7)	0.0053(8)	0.0068(8)	0.0081(8)	0.093(7)
y (M3)	0.3084(1)	0.3086(2)	0.3082(1)	0.3081(1)	0.3083(1)
z (M3)	0.1181(1)	0.1182(2)	0.1179(1)	0.1182(1)	0.1181(1)

[a] Atom positions: Ba1 2a 0,0,0; Ba2 6d 0,1/4,1/2; M1 6c 1/4,0,1/2; M2 16i x,x,x; M3 24k 0,y,z. Occupations of M1, M2 and M3 are each fixed at 34.78% Ga and 65.21% Ge.

tions were averaged in the cubic space group $Pm\bar{3}n$. For each temperature, approximately 1200 reflections were measured, leading to about 200 independent reflections with $F_{obs}/(\sigma F)>3$, and a data to parameter ratio greater than 11. Observed structure factors were used in least-squares refinement of the scale factor, atom positional parameters, and anisotropic atomic displacement parameters. The coherent scattering lengths used were: Eu-153 (8.22 fm), Ba (5.07 fm), Ge (8.19 fm), and Ga (7.29 fm) [19]. A Becker and Coppens Type I extinction correction

was refined [20]. For fitting the magnetic structure of $Eu_8Ga_{16}Ge_{30}$ for the temperatures below 40 K, the crystal symmetry was lowered to $P1$ to allow the Eu moments to take on any orientation, and the unaveraged data were used. The analytical approximation to the $\langle j_0 \rangle$ magnetic form factor for Eu^{2+} was taken from Brown [21]. Tables 1 and 2 summarize the refinement results for $Ba_8Ga_{16}Ge_{30}$ and $Eu_8Ga_{16}Ge_{30}$, respectively. Anisotropic atomic displacement parameters will be deposited in the Inorganic Crystal Structure Database.

Table 2
Refinement results for $Eu_8Ga_{16}Ge_{30}$, $Pm\bar{3}n$, $Z=1$, 24k split-site model from neutron single-crystal diffraction data[a]

Temperature (K)	12[b]	25[b]	40	80	120	160	200	295
Measured reflections	1118	1112	1143	1143	1143	1143	1144	2558
Independent reflections	1118	1112	428	428	428	428	428	441
Reflections with $I>3\sigma(I)$	640	634	285	293	295	280	279	298
Number of parameters	3	3	18	18	18	18	18	18
$R(F)$	0.083	0.080	0.054	0.049	0.057	0.051	0.053	0.027
$wR(F^2)$	0.158	0.156	0.1094	0.090	0.102	0.093	0.101	0.055
Goodness-of-fit, S	2.396	2.409	2.021	1.892	2.165	1.914	2.045	1.502
Extinction coefficient ($\times 10^{-5}$)	15(1)	15(1)	10(1)	8.5(1)	10(5)	7(1)	7(1)	9.4(7)
Cell a (Å)	10.6695(2)	10.6702(2)	10.6706(2)	10.6707(6)	10.6747(6)	10.6766(6)	10.6806(6)	10.6886(8)
$\rho_{calc.}$ (g/cm^3)	6.164	6.164	6.162	6.155	6.155	6.152	6.145	6.131
Eu magnetic moment (μ_B)	5.6(2)	3.9(2)	–	–	–	–	–	–
U_{eq} (Eu1) (Å^2)	0.0089	0.0089	0.0021(7)	0.0035(7)	0.0056(9)	0.0066(8)	0.0074(9)	0.0127(5)
U_{eq} (Eu2) (Å^2)	0.0135	0.0135	0.025(5)	0.024(3)	0.028(6)	0.031(6)	0.037(8)	0.042(3)
y (Eu2)	0.250	0.250	0.250(1)	0.253(1)	0.250(1)	0.251(1)	0.257(1)	0.257(1)
z (Eu2)	0.5411	0.5411	0.5411(8)	0.5421(8)	0.540(1)	0.540(1)	0.540(1)	0.5367(6)
U_{eq} (M1) (Å^2)	0.0073	0.0073	0.0065(9)	0.006(1)	0.007(1)	0.0091(9)	0.009(1)	0.0131(5)
U_{eq} (M2) (Å^2)	0.0045	0.0045	0.0045(5)	0.0050(5)	0.0058(6)	0.0069(5)	0.0079(6)	0.0110(3)
x (M2)	0.1839	0.1839	0.18390(8)	0.18396(8)	0.1841(1)	0.18398(9)	0.1838(1)	0.18398(5)
U_{eq} (M3) (Å^2)	0.0046	0.0046	0.0049(6)	0.0058(5)	0.0066(7)	0.0073(6)	0.0086(7)	0.0118(3)
y (M3)	0.3091	0.3091	0.3091(1)	0.3091(1)	0.3092(1)	0.3092(1)	0.3092(1)	0.30914(7)
z (M3)	0.1167	0.1167	0.1167(1)	0.1168(1)	0.1167(1)	0.1168(1)	0.1166(1)	0.11687(6)

[a] Atom positions: Eu1 2a 0,0,0; Eu2 24k 0,y,z; M1 6c 1/4,0,1/2; M2 16i x,x,x; M3 24k 0,y,z. Occupations of M1, M2 and M3 are each fixed at 34.78% Ga and 65.21% Ge; the split Eu2 site is 25% occupied.

[b] These refinements, made in $P1$ space group symmetry, include magnetic scattering from the Eu atoms ferromagnetically aligned along (100), with the atomic positions fixed at the 40 K values and the atomic displacement parameters fixed at extrapolated values from above T_c.

3. Results

For the structure refinements, the starting model was taken from the room-temperature X-ray refinement $Ba_8Ga_{16}Ge_{30}$ reported by Eisenmann et al. [8]. The structure has two distinct sites for the divalent atoms and the cage framework contains three distinct metal sites occupied by Ge and Ga (Fig. 1). The distribution of the Ge and Ga over the framework sites is not easily determined using conventional X-ray diffraction data; but for neutron diffraction data, the scattering lengths are sufficiently different, 12%, that various site occupancy models can be tested and compared. Similar to $Sr_8Ga_{16}Ge_{30}$ [6] the fully disordered model, i.e. 34.78%Ga:65.22%Ge on each metal site, gives the best overall fit in each case.

3.1. $Ba_8Ga_{16}Ge_{30}$

From the refinements, the atomic displacement parameter for Ba2 is large and anisotropic. Moreover, the anisotropy of the Ba2 displacement parameters indicates a much smaller amplitude in the $\langle 100 \rangle$ directions than in the perpendicular directions. The temperature dependence of the isotropic equivalent displacement (U_{eq}) parameters for Ba1 and the other three metal sites are similar and all have the expected behavior (Fig. 2a). The U_{eq} of the Ba2 site has less temperature dependence (Fig. 2c) and does indicate some positional disorder as compared to Ba1. Nevertheless, the refinements (Table 1) agree reasonably well with the previous work of Eisenmann et al. [8]. With the Ba2 at the large cage center, the $6d$ $0,1/4,1/2$ position, the 24 near-neighbor distances range between 3.628(1) and 4.166(2) Å with a mean of 3.874 Å. Despite the presence of (Ga,Ge) solid solution, this is still significantly longer than the mode of 3.55 Å for the distribution of 340 Ba–Ge distances taken from 21 binary and ternary compounds in the Inorganic Crystal Structure Database. The nuclear density in the large cage is nicely spherical and sharply peaked at the cage center; see Keppens et al. [12] and Sales et al. [17] for the Fourier difference maps. For Ba1 at the small cage center, $2a$ $0,0,0$ position, the 20 near-neighbor atoms are either 3.471(2) or 3.588(1) Å away, with a mean of 3.541 Å, which is what would be expected given the observed Ba–Ge distance distribution. In the single-site model, the minimum separation between near-neighbor Ba2 atoms is simply given by $a/2$ or 5.39 Å.

3.2. $Eu_8Ga_{16}Ge_{30}$

The initial refinements indicated full occupancy for both Eu sites and that the isotropic atomic displacement parameter for Eu2 was even larger than that of Sr2 in $Sr_8Ga_{16}Ge_{30}$ [6] (Fig. 2c), for which a fractionally occupied split atom site was explored to refine the structural model. Whereas, for the $Sr_8Ga_{16}Ge_{30}$ case, the quality of
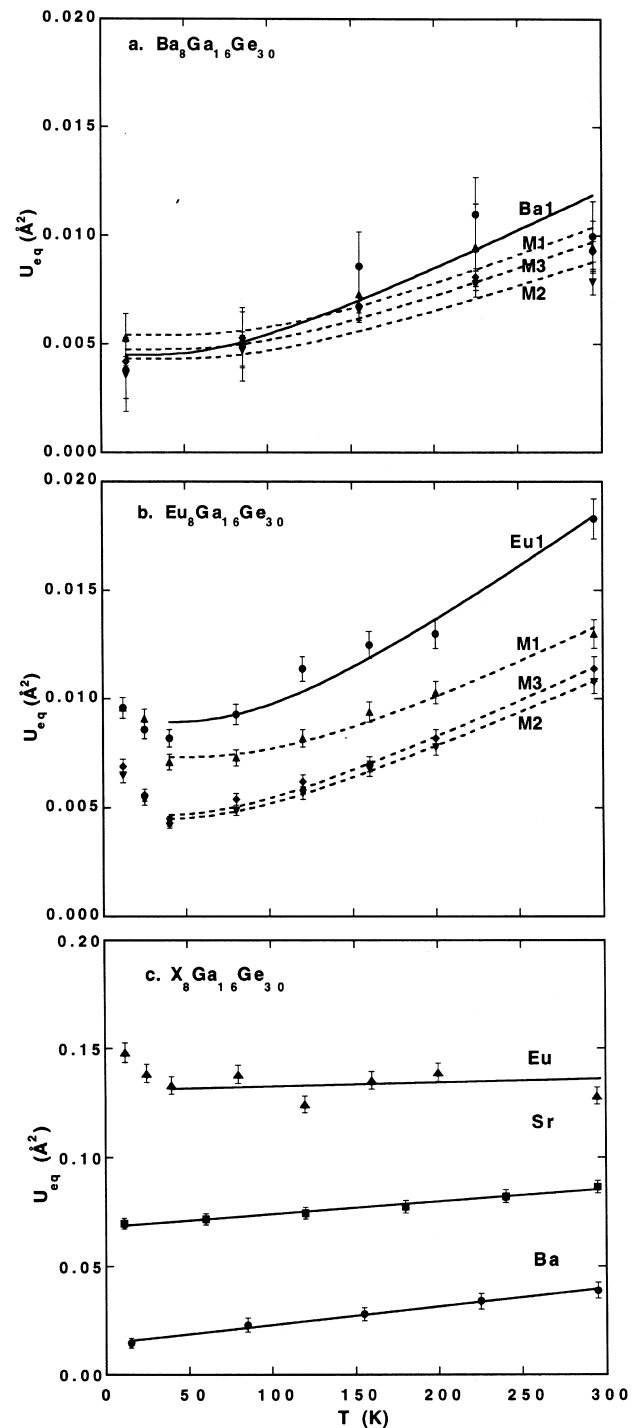

Fig. 2. a. Temperature dependence of the equivalent isotropic displacement parameters (single Eu2 site model) for the X1 and M sites of (a) $Eu_2Ga_{16}Ge_{30}$ and (b) $Ba_2Ga_{16}Ge_{30}$. The regression fits are for $a \coth(b/T)$, where a and b are the fitting parameters. Below 40 K in the case of the $Eu_2Ga_{16}Ge_{30}$ the refinement model does not include any magnetic scattering, so therefore the U_{eq} values deviate from the expected low temperature behavior, i.e. the U values try to account for the magnetic scattering contribution. (c) Temperature dependence of the equivalent isotropic displacement parameters (single X2 site model) for the X2 sites in $Eu_2Ga_{16}Ge_{30}$, $Sr_2Ga_{16}Ge_{30}$, and $Ba_2Ga_{16}Ge_{30}$. The apparent $U(T)$ is large for X2 in the single-site model, and implies that the static disorder progressively increases from Ba to Sr to Eu. The $Sr_2Ga_{16}Ge_{30}$ data are from Chakoumakos et al. [6].

the refinements was essentially the same for either the split-site or single-site structural models, for $Eu_8Ga_{16}Ge_{30}$ the split-site model significantly improves the quality of the refinement. If we assume the Eu2 atom is disordered over the split-atom positions and the average symmetry remains $Pm\bar{3}n$, a 4-fold splitting of the cage-centered Eu2 sites $(0,1/4,1/2)$ can be accomplished simply by fractionally occupying either of the $24k$ $(0,y,z)$ or $24j$ $(y+1/2,1/4,y)$ Wyckoff sites adjacent to the cage center position. Of these two possibilities, the $24k$ position gives a better refinement. These final refinement results, using anisotropic displacement parameters on all of the atoms, are given in Table 2. The split-sites are moved off from the cage center by 0.4 Å, and this value remains essentially the same at all temperatures studied. Displacement ellipsoids for the split Eu2 site and the atoms making up the large cage are shown in Fig. 1.

From the temperature dependence of the isotropic displacement parameters for $Eu_8Ga_{16}Ge_{30}$ (Fig. 2b,c) the apparent $U(T)$ for Eu2 for the single-site model is enormous and temperature-independent. This implies an extremely large positional disorder by the magnitude of the low temperature intercept (Fig. 2c), particularly as it compares to the $U(T)$ for Eu1 (Fig. 2b). With Eu2 fractionally occupying the split site, its U_{eq} value is dramatically reduced, but still is the largest of all the atoms in the crystal. Splitting the site effectively accounts for most of the apparent positional disorder, bringing $U(T)$ down to about the same level as that of Ba2 in $Ba_8Ga_{16}Ge_{30}$. The U_{eq} for the Eu1 site is also large, but more on par with the Ga,Ge sites due to its smaller sized coordination environment.

Difference Fourier maps of the Eu2 site, for which the Eu2 atom was removed from the structural model, clearly show the residual nuclear density to have distinct peaks in the directions of the $24k$ split-site positions and significantly less density at the cage center position (Fig. 3a). In cross-section, this nuclear density has a rough toroidal shape (Fig. 3b).

Below 35 K, $Eu_8Ga_{16}Ge_{30}$ orders ferromagnetically. Magnetization measurements on a portion of the same single crystal as used for the neutron diffraction experiments are reported in [17]. The saturation magnetization corresponds to a magnetic moment per Eu ion of 7 μ_B (the free ion value). The field dependence of the magnetization showed little hysteresis, implying that $Eu_8Ga_{16}Ge_{30}$ is a soft ferromagnet with a small coercive field of order 1–10 gauss. The structure factor amplitudes for low angle reflections, which include magnetic scattering contributions, clearly increase with decreasing temperature, as compared to high angle reflections with no magnetic contribution (Fig. 4). If one neglects the magnetic scattering contribution in the structure refinements, the atomic displacement parameters try to correct for the additional intensity at low scattering angles, which causes the upturn of the U_{eq} values below 40 K evident in Fig. 2b,c.

In order to include the magnetic scattering in the structure refinements for the 12 and 25 K data, several preliminary steps were made. Working from the split-site model previously described, the $U_{ij}(T)$ values for each atom were fit by the expression $U = a\coth(b/T)$ and low temperature values extrapolated. These $U_{ij}(T)$ values were held fixed in subsequent refinements. The crystal symmetry was lowered to $P1$ so that the Eu moment vectors could take on any orientation, and the atom positions were fixed at the 40 K values. The magnetic moments on the Eu1 and Eu2 atoms were constrained to be equal, and several principal directions were examined for the moment vector orientations to determine the best fit to the data. In this manner, it was determined that the magnetization is directed along the (100) direction. The refined moment for each Eu atom and the quality of the least-squares fits are given in Table 2 for the 12 and 25 K data. The Eu magnetic moment is not fully saturated at these temperatures, but the moment decreases as T_c is approached following the typical power law behavior. The minimum Eu···Eu separation is 5.335 Å in $Eu_8Ga_{16}Ge_{30}$, which is similar to that of 5.144 Å in EuO, and much smaller than 7.93 Å in the filled skutterudite $EuFe_4Sb_{12}$ [22,23], but both of which exhibit similar ferromagnetic behavior.

4. Discussion

Previously [4,5,7], we have shown how the $U(T)$ data for a crystal can be used to estimate its Debye temperature, average velocity of sound, and lattice thermal conductivity. The $U(T)$ data also can be used to describe the localized vibration of a loosely bound 'rattling' atom by means of an Einstein oscillator model. The motivation for these interests has been to provide estimates of quantities, such as the lattice thermal conductivity, important for evaluating candidate thermoelectric materials, such as the semiconducting clathrates. In themselves, the semiconducting clathrates are ideal to study the microscopic origin of glass-like heat conduction in crystalline solids; however, an important question remains not fully answered. Why do certain 'rattlers' produce a glass-like thermal conductivity, while others only lower the thermal conductivity? The $X_8Ga_{16}Ge_{30}$ (X=Eu, Sr, Ba) compounds might begin to help us understand this question, because we observe thermal conductivities typical both of a crystal (Ba) and a glass (Sr, Eu) [17]. For decreasing size of the guest atom, Ba>Sr>Eu, several structural and physical properties change systematically: (1) the apparent U_{eq} and static positional disorder of the guest atom in the large cage increase markedly; (2) the temperature dependence of U actually appears to decrease slightly; (3) from the Fourier mapping of the nuclear density within the large cavity and the structure refinements using split-site models for the large cavity occupant, the probability increases for finding the guest atom increasingly further away from the cage
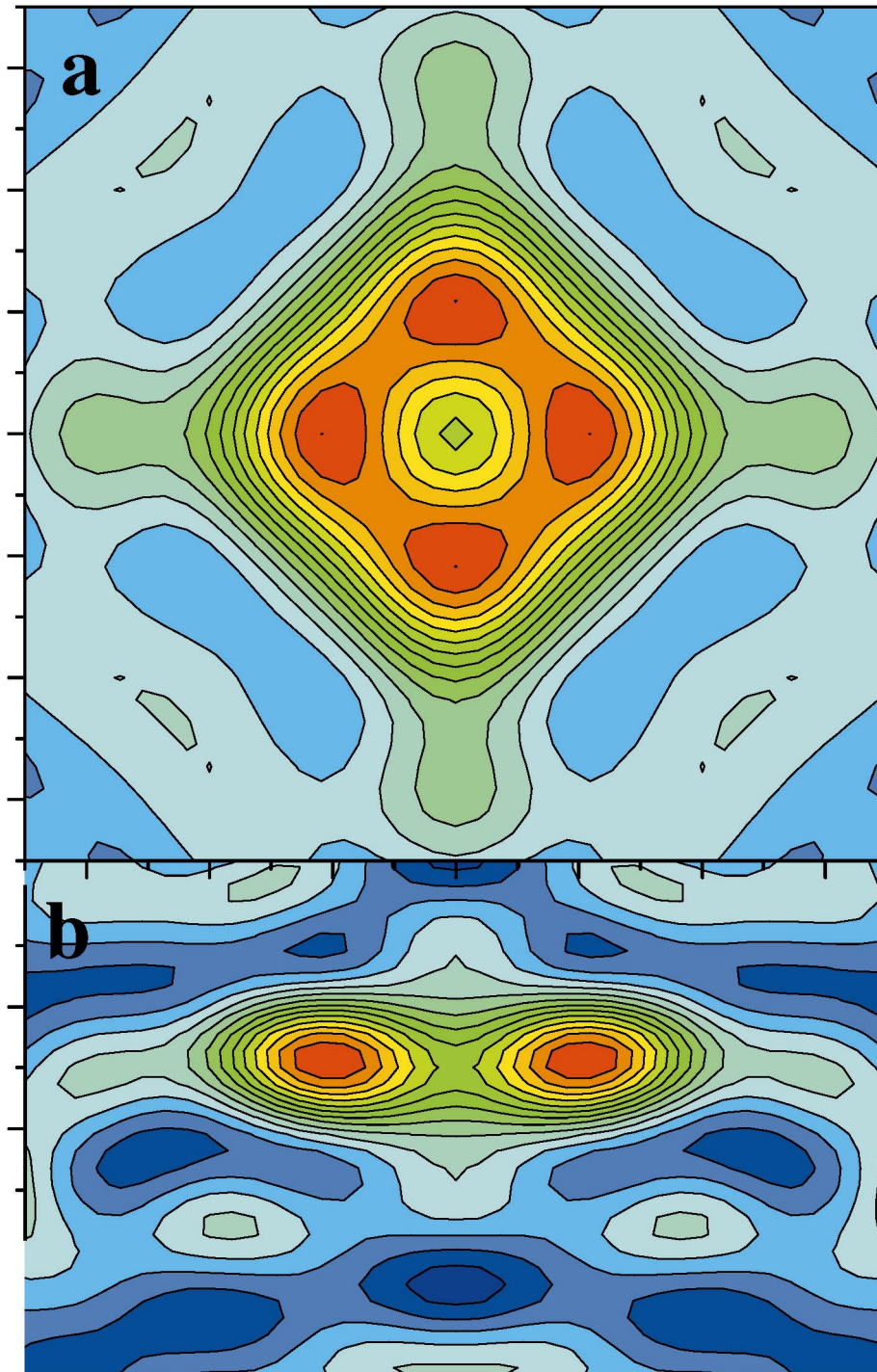
Fig. 3. (a) A 100 section of the difference Fourier map of the Eu2 site, where the Eu2 atom has been removed from the structural model. The difference nuclear density at the Eu2 site has distinct lobes in the directions of the 24k sites. The map size is 2.5 Å^2, and the contour interval is 0.1 fm/Å^3 (drawn for -0.3 to 1.3 fm/Å^3). (b) Perpendicular section to that in (a) shows that the nuclear density is actually somewhat doughnut-shaped.

center position; (4) from low temperature heat capacity measurements the approximate Einstein oscillator temperature of the atom in the large cage decreases, from 60 to 53 to 30 K, respectively [17]; and (5) the thermal conductivity changes from crystal-like to glass-like and continues to decrease [12,17]. At first glance, (2) and (4) seem con-

tradictory; however, the modeling of the heat capacity data does not provide a means to separate the static and dynamic contributions to the mean square atomic displacements. Low temperature (<1 K) thermal conductivity data indicate the possibility of localized tunnel states in $Sr_8Ga_{16}Ge_{30}$ [12,24]; therefore, the nuclear density maps
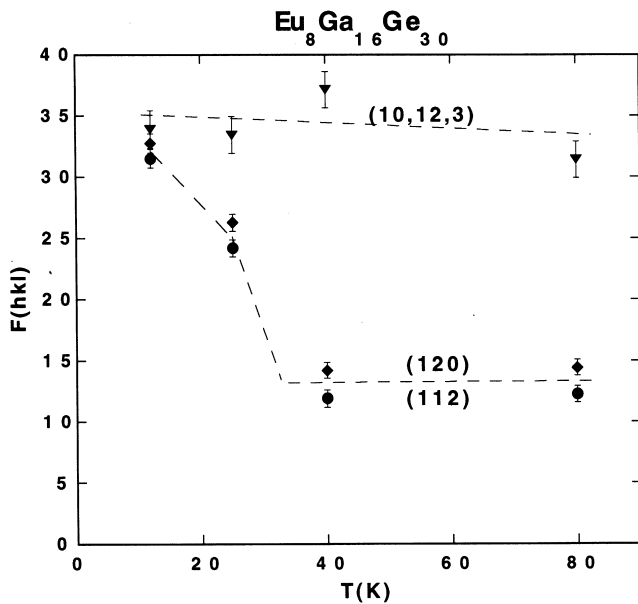
Fig. 4. Comparison of the temperature dependence of $F(hkl)$ for two low-angle reflections, affected by the magnetism, and a high-angle nuclear peak with essentially no magnetic contribution.

derived from Fourier synthesis of the neutron diffraction data may represent an averaged picture of the tunneling states in the $Sr_8Ga_{16}Ge_{30}$ and $Eu_8Ga_{16}Ge_{30}$ crystals. This viewpoint also supports the idea that both rattling and tunneling states are necessary to produce a true glass-like thermal conductivity. Intuitively, this makes sense in that the host framework atoms constitute the crystal, while the positionally disordered atoms in the large cages constitute the glass.

5. Conclusions

The atomic displacement parameters for the Eu2 site in $Eu_8Ga_{16}Ge_{30}$ are anomalously large over the entire temperature range, 10–300 K, implying a large positional disorder associated with the Eu2 site. The anisotropy of the Eu2 displacements are also large and the site is better described by a fractionally occupied 4-fold split-site, which effectively accounts for most of the positional disorder. When refinements are carried out with a split-site model, the refined Eu2 atom position is about 0.4 Å away from the cage center position $(0,1/4,1/2)$ in the z-direction. Whereas, in the case of $Sr_8Ga_{16}Ge_{30}$ the refinements using the split-site model have about the same agreement as refinements using the single site model, in the $Eu_8Ga_{16}Ge_{30}$ case, the split-site model is significantly better. Moreover, the split-site model using the $24k$ positions is better than that using the $24j$ positions. Difference Fourier maps of the anomalous Eu site corroborate this description by revealing residual nuclear density

in the large cage with distinct peaks in the directions of the split-atom positions. Furthermore, we see no evidence for a superlattice or other indications of a reduced crystal symmetry at low temperatures, possibly due to the Eu atoms preferentially locking into off-center positions; although we have not made a concerted effort to do so, for instance, by using an area detector.

Below 35 K, $Eu_8Ga_{16}Ge_{30}$ orders ferromagnetically, with the magnetization directed along (100). The temperature dependence of the refined Eu magnetic moments at 25 and 12 K exhibit typical power law behavior, and project a saturation value, 7 μ_B, equal to the free ion value.

Acknowledgements

References

[1] B.C. Sales, D. Mandrus, R.K. Williams, Science 272 (1996) 1325.
[2] B.C. Sales, D. Mandrus, B.C. Chakoumakos, V. Keppens and J.R. Thompson Phys, Rev. B 56 (1997) 15081.
[3] G.D. Mahan, B.C. Sales, J. Sharp, Phys. Today March (1997) 42.
[4] B.C. Sales, B.C. Chakoumakos, D. Mandrus, J.W. Sharp, N.R. Dilley, M.B. Maple, in: T.M. Tritt, M.G. Kanatzidis, G. Mahan, H.B. Lyon Jr. (Eds.), Thermoelectric Materials 1998 — The Next Generation Materials for Small-Scale Refrigeration and Power Generation Applications, Materials Research Society Symposium Proceedings 545, Materials Research Society, Pittsburgh, PA, 1998, p. 13.
[5] B.C. Sales, B.C. Chakoumakos, D. Mandrus, J.W. Sharp, J. Solid State Chem. 146 (1999) 528.
[6] B.C. Chakoumakos, B.C. Sales, D. Mandrus, G.S. Nolas, J. Alloys Comp. 296 (2000) 80.
[7] B.C. Sales, D.G. Mandrus, B.C. Chakoumakos, in: T.M. Tritt (Ed.), Recent Trends in Thermoelectric Materials Research II, Semiconductors and Semimetals, Vol. 70, Academic Press, San Diego, CA, 2001, p. 1.
[8] B. Eisenmann, H. Schäfer, R. Zakler, J. Less-Common Met. 118 (1986) 43.
[9] J.S. Kasper, P. Hagenmuller, M. Pouchard, C. Cros, Science 150 (1965) 1713.
[10] G.S. Nolas, J.L. Cohn, G.A. Slack, S.B. Schujman, Appl. Phys. Lett. 73 (1998) 178.
[11] G.S. Nolas, in: T.M. Tritt, M.G. Kanatzidis, G. Mahan, H.B. Lyon Jr. (Eds.), Thermoelectric Materials 1998 — The Next Generation Materials for Small-Scale Refrigeration and Power Generation Applications, Materials Research Society Symposium Proceedings 545, Materials Research Society, Pittsburgh, PA, 1998, p. 435.
[12] V. Keppens, B.C. Sales, D. Mandrus, B.C. Chakoumakos, C. Laermans, Phil. Mag. Lett. 80 (2000) 807.
[13] J.L. Cohn, G.S. Nolas, V. Fessatidis, T.H. Metcalf, G.A. Slack, Phys. Rev. Lett. 82 (1999) 779.

[14] R. Kröner, Zintl-Phasen der Alkalimetalle und des Bariums mit Clathratstruktur, Dissertation, Universität Stuttgart, Germany, 1989.

[15] H.G. von Schnering, R.R. Kröner, H. Menke, K. Peters, R. Nesper, Z. Kristallogr. (New Crystal Struct.) 213 (1998) 677.

[16] J.-T. Zhao, J.D. Corbett, Inorg. Chem. 33 (1994) 5721.

[17] B.C. Sales, B.C. Chakoumakos, R. Jin, J.R. Thompson, D. Mandrus, Phys. Rev. B, in press.

[18] A.C. Larson, R.B. Von Dreele, GSAS, Generalized Structure Analysis System, Los Alamos National Laboratory Report, 1986–2000, LAUR 86-748.

[19] V.F. Sears, Neutron News 3 (1992) 26.

[20] P.J. Becker, P. Coppens, Acta Crystallogr. A30 (1974) 129.

[21] P.J. Brown, in: A.J.C. Wilson (Ed.), International Tables for Crystallography, Vol. C, Kluwer, Boston, MA, 1992, p. 391.

[22] C.B.H. Evers, W. Jeitschko, L. Boonk, D.J. Braun, T. Ebel, U.D. Scholz, J. Alloys Comp. 224 (1995) 184.

[23] M.E. Danebrock, C.B.H. Evers, W. Jeitschko, J. Phys. Chem. Solids 57 (1996) 381.

[24] V. Keppens, D. Mandrus, B.C. Sales, B.C. Chakoumakos, P. Dai, R. Coldea, M.B. Maple, D.A. Gajewski, E.J. Freeman, S. Bennington, Nature 395 (1998) 876.